Global emergence of Carbapenem-resistant Hypervirulent *Klebsiella pneumoniae* driven by an IncFII$_{K34}$ KPC-2 plasmid

Jianping Jiang,[a,b,m] Leilei Wang,[a,m] Yiyi Hu,[a] Xin Chen,[a] Pei Li,[a] Jianfeng Zhang,[a] Yixin Zhang,[a] Jiachun Su,[a] Xiaogang Xu,[a] Yonghong Xiao,[c] Zhengyin Liu,[d] Yunsong Yu,[e] Hainv Gao,[f] Yohei Doi,[g,h] David van Duin,[i] Vance G. Fowler, Jr.,[j,k] Liang Chen,[b,l,**] and Minggui Wang[a,*]

[a]Institute of Antibiotics, Huashan Hospital, Fudan University, and Key Laboratory of Clinical Pharmacology of Antibiotics, National Heath Commission of the People's Republic of China, Shanghai, China
[b]Center for Discovery and Innovation, Hackensack Meridian Health, Nutley, NJ, USA
[c]State Key Laboratory for Diagnosis and Treatment of Infectious Diseases, The First Affiliated Hospital of Medical School of Zhejiang University, Hangzhou, China
[d]Infectious Disease Section, Department of Internal Medicine, Peking Union Medical College Hospital, Beijing, China
[e]Department of Infectious Diseases, Sir Run Run Shaw Hospital, Zhejiang University School of Medicine, Hangzhou, China
[f]Department of Infectious Diseases, Key Laboratory of Artificial Organs and Computational Medicine of Zhejiang Province, Shulan (Hangzhou) Hospital, Shulan International Medical College, Zhejiang Shuren University, Hangzhou, China
[g]Division of Infectious Diseases, University of Pittsburgh School of Medicine, Pittsburgh, PA, USA
[h]Departments of Microbiology and Infectious Diseases, Fujita Health University School of Medicine, Aichi, Japan
[i]Division of Infectious Diseases, University of North Carolina, Chapel Hill, NC, USA
[j]Division of Infectious Diseases, Department of Medicine, Duke University Medical Center, Durham, NC, USA
[k]Duke Clinical Research Institute, Duke University School of Medicine, Durham, NC, USA
[l]School of Pharmacy and Pharmaceutical Sciences, University at Buffalo, Buffalo, NY, USA

eBioMedicine
2025;113: 105627
Published Online xxx
https://doi.org/10.1016/j.ebiom.2025.105627

Summary

Background Carbapenem-resistant hypervirulent *Klebsiella pneumoniae* (CR-hvKp) has been increasingly reported worldwide, posing a severe challenge to public health; however, the mechanisms driving its emergence and global dissemination remain unclear.

Methods We analysed CR-hvKp strains derived from canonical hvKp backgrounds, and acquired a carbapenemase-encoding gene. These strains were identified from 485 CRKp isolates in the CRACKLE-2 China cohort, 259 CRKp isolates from a multi-centre study, and 67,631 *K. pneumoniae* genomes available in GenBank. Clinical isolates harbouring the IncFII$_{K34}$ KPC-2 plasmid were selected for genome sequencing, RNA-Seq, conjugation assays, in vivo, ex vivo, and in vitro phenotypic characterisation.

Findings Analysis of clinical CR-hvKp isolates and the 414 genomes from 24 countries available in GenBank identified an IncFII$_{K34}$ KPC-2 plasmid as the prevalent KPC plasmid (detected in 25%, 45/178 of KPC-producing CR-hvKp). Compared with the epidemic IncFII$_{K2}$ KPC-2 plasmid, the IncFII$_{K34}$ KPC-2 plasmid exhibited a 100- to 1000-fold increase in conjugation frequency (10^{-4}–10^{-5} vs. 10^{-7}) and an in vitro growth advantage under meropenem challenge–likely due to the overexpression of conjugation-related genes and an increased *bla*$_{KPC}$ copy number and expression. CR-hvKp isolates and hvKp transconjugants carrying this plasmid often exhibited reduced mucoviscosity, while retaining hypervirulence in both murine models and human neutrophil assays.

Interpretation The IncFII$_{K34}$ plasmid may be a key factor driving the global dissemination of CR-hvKp, underscoring the urgent need for enhanced molecular surveillance of this emerging pathogen.

Funding National Natural Science Foundation of China and National Institutes of Health.

Keywords: hvKp; CR-hvKp; IncFII$_{K34}$; *bla*$_{KPC-2}$-carrying plasmid

*Corresponding author. Institute of Antibiotics, Huashan Hospital, Fudan University, No. 12 Wulumuqi Road, Shanghai, China.
**Corresponding author. School of Pharmacy and Pharmaceutical Sciences, University at Buffalo, Buffalo, NY, USA.
E-mail addresses: mgwang@fudan.edu.cn (M. Wang), liangch@buffalo.edu (L. Chen).
[m]These authors contributed equally to this work.

Research in context

Evidence before this study

We conducted a comprehensive PubMed search without language restrictions for articles published prior to August 17, 2024, using keywords "Carbapenem resistant", "Hypervirulent", and "*Klebsiella pneumoniae*". The search primarily yielded studies focussing on the epidemiology and characterisation of ST11 carbapenem-resistant *K. pneumoniae* strains that had acquired hypervirulence plasmid (Hv-CRKp). Notably, research on carbapenem-resistant hypervirulent *K. pneumoniae* (CR-hvKp) strains, particularly canonical hvKp lineages of ST23, ST86, and ST65 that acquired carbapenem resistance, is limited. One study provided a genomic epidemiological characterisation of carbapenem-resistant and hypervirulent *K. pneumoniae* in China. Among the 784 bla_{KPC-2}-bearing CRKp strains, six ST86 CR-hvKp strains were identified. Phenotypic characterisation underscored that, despite the rapid increase and prevalence of ST11 Hv-CRKp strains carrying the virulence plasmid, the majority did not exhibit hypervirulent phenotypes. Another study reported an outbreak of KPC-2-encoding ST23 and ST65 CR-hvKp strains in Singapore in 2010–2015. Other cases of CR-hvKp isolates have been reported sporadically. For example, one KPC-2-encoding ST23 CR-hvKp strain was reported from the United States in 2019; two KPC-2-encoding ST86 CR-hvKp strains were reported from Canada in 2019; one OXA-48-producing ST86 CR-hvKp strain was reported from France in 2020 and one OXA-232-producing ST23 CR-hvKp strain was reported from India in 2020. A recent study documented the emergence of a conjugative plasmid formed through the fusion of a non-conjugative pK2044-like plasmid with a conjugative KPC-2 plasmid in ST86 CR-hvKp. Nevertheless, understanding of the formation and spread of CR-hvKp is still limited.

Added value of this study

In this study, we analysed all available genome sequences of canonical CR-hvKp strains from two multi-centre studies and the NCBI GenBank, and identified an $IncFII_{K34}$ KPC-2 plasmid that predominates among CR-hvKp. The plasmid was found in *K. pneumoniae* reported from 33 countries. We found that the $IncFII_{K34}$ KPC-2 plasmid exhibited high conjugation frequency due to the elevated expression of conjugation-associated genes. Furthermore, the plasmid provided CR-hvKp a survival advantage over the $IncFII_{K2}$ KPC-2 plasmid harbouring CR-hvKp under carbapenem exposure, which may be conferred by increased bla_{KPC-2} expression. These discoveries bring valuable insights to our current understanding of the formation and spread of CR-hvKp, which is rapidly becoming a global public health concern.

Implications of all the available evidence

Building upon prior evidence, our study underscores the emergence and prevalence of an $IncFII_{K34}$ KPC-2 plasmid in CR-hvKp. The noteworthy characteristics of this plasmid, including its high conjugation rate and elevated carbapenem resistance, highlight the critical importance of global surveillance of the $IncFII_{K34}$ KPC-2 plasmids and CR-hvKp strains.

Introduction

Hypervirulent *Klebsiella pneumoniae* (hvKp) causes severe community-associated infections like liver abscesses and meningitis in otherwise healthy individuals, leading to high mortality rates.[1] Of particular concern is the emergence of carbapenem-resistant hvKp (CR-hvKp) that shows resistance to most clinically available β-lactams, greatly limiting treatment options.[2] On July 31, 2024, the World Health Organization reported a rising global incidence of CR-hvKp, particularly of sequence type (ST) 23.[3] Furthermore, inadequate laboratory capacity for detecting these strains has likely resulted in a substantial underestimation of the true global burden of both hvKp and CR-hvKp.

Compared with classic carbapenem-resistant *K. pneumoniae* (CRKp) strains, such as those from ST11 and ST15 that have acquired hypervirulence plasmids (the primary virulence factor of hvKp), canonical hvKp strains like ST23, ST86, and ST65 that have acquired resistance plasmids encoding a carbapenemase gene exhibit significantly higher virulence,[4] warranting greater attention. For instance, a study of 784 bla_{KPC-2}-bearing CRKp strains in China revealed that, although ST11 Hv-CRKp strains carrying the virulence plasmid are rapidly increasing in prevalence, most do not exhibit hypervirulent phenotypes.[5]

Several factors are thought to constrain the formation and spread of CR-hvKp strains. One primary factor is the hypermucoviscosity of hvKp strains, which reduces the likelihood of carbapenemase-encoding plasmids entering the cells.[6] Another factor is the incompatibility between carbapenemase-encoding plasmids and hvKp strains, which makes hvKp strains susceptible to carbapenems.[7] Additionally, the chromosome-borne type I-E CRISPR-Cas system may restrict the transfer and maintenance of carbapenemase-encoding plasmids in ST23 hvKp strains.[8]

Despite these barriers, various carbapenemase-encoding plasmids have been identified in the recent global spread of CR-hvKp. For example, an $IncFII_{K2}$ KPC-2 plasmid that originated from the prototypical pKPQIL plasmid was identified in an ST23 CR-hvKp strain from the United States in 2019[9]; an $IncFII_{K21}$ KPC-2 plasmid was found in two ST86 CR-hvKp strains from Canada in 2019[10]; a nontypable KPC-2 plasmid was reported in three ST23 CR-hvKp strains collected from a

patient in Singapore in 2020[11]; and an IncP1 KPC-2 plasmid was documented in one ST23 CR-hvKp strain from China in 2021.[12] Additionally, other carbapenemase-encoding plasmids, such as an IncL OXA-48 plasmid in an ST86 CR-hvKp strain from France[13] and a ColKP3 OXA-232 plasmid in an ST23 CR-hvKp strain from India,[14] have been reported. Notably, a recent study documented the emergence of a conjugative plasmid formed through the fusion of a non-conjugative pK2044-like plasmid with a conjugative KPC-2 plasmid in ST86 CR-hvKp.[15]

However, these reports remain largely sporadic, and it is unclear how common these plasmids are within the broader CR-hvKp population. While carbapenemase-encoding plasmids play a crucial role in the spread of CRKp clones (e.g., IncFII$_{K2}$ KPC plasmids bolstering ST11 and ST258),[16] their role in CR-hvKp dissemination is less well understood. Investigating how these plasmids overcome the barriers to establish themselves in hvKp is essential for improving our knowledge of CR-hvKp formation and dissemination.

In this study, we identified an IncFII$_{K34}$ KPC-2 plasmid in CR-hvKp clinical isolates, which was prevalent in the 414 CR-hvKp genomics currently available in GenBank. This plasmid appears to play a key role in overcoming the barriers typically restricting CR-hvKp formation and may be driving its global spread. These discoveries advance our understanding of the evolution of CR-hvKp and underscore the importance of monitoring CR-hvKp in both clinical and environmental settings.

Methods

Identification of the carbapenemase-encoding plasmid in canonical hvKp-derived CR-hvKp

In this study, CR-hvKp was defined as canonical hvKp-derived CR-hvKp strains, belonging to ST23, ST86, or ST65, and harbouring both a pK2044-like virulence plasmid and a carbapenemase gene. A total of 485 and 259 CRKp clinical isolates from two previous multicentre studies were genomically screened for canonical CR-hvKp.[17,18] A nontypeable IncFII$_K$ allele was compared with 33 known alleles in the plasmid MLST database and submitted as IncFII$_{K34}$. All complete IncFII$_K$ plasmids from PLSDB 2021_06_23_v2[19] were analysed. A total of 67,631 *K. pneumoniae* genomes, each with fewer than 400 contigs and a genome size between 4.5 Mbp and 6.5 Mbp, were retrieved from the NCBI GenBank (accessed on August 12, 2024) to assess the prevalence of CR-hvKp and the distribution of IncFII$_{K34}$ plasmid.

Conjugation of KPC-2 plasmids and antimicrobial susceptibility testing

Conjugation experiments were conducted using the filter-mating method. In the conjugation of *bla*$_{KPC-2}$ plasmids from the donors CR-hvKp (*K. pneumoniae* H39, DD02357, DD01665, and DD02201) and CRKp (*K. pneumoniae* HS11286), the sodium azide-resistant *E. coli* J53 was used as the recipient. Transconjugants were selected on Luria–Bertani (LB) agar plates supplemented with meropenem (0.5 μg/mL) and sodium azide (100 μg/mL). In the conjugation of *bla*$_{KPC-2}$ plasmids from the donors (J53::pKPC-H39, J53::pKPC-DD02357, J53::pKPC-DD01665, J53::pKPC-DD02201, and J53::pKPC-HS11286), *K. pneumoniae* NTUH-K2044 (dipotassium tellurite-resistance due to the presence of *ter* operon) was used as the recipient. Transconjugants were selected on LB agar plates supplemented with meropenem (0.5 μg/mL) and dipotassium tellurite (3 μg/mL). Twenty-four colonies were randomly selected for each transconjugant and tested for mucoviscosity using low-speed centrifugation, followed by the measurement of OD$_{600}$ values of the supernatant. Six transconjugants colonies with reduced mucovisity were selected for PCR amplification of *rmpA* and *wzc* genes, followed by Sanger sequencing. In the conjugation of hypervirulence plasmids from the donors (NTUH-K2044::pKPC-H39, NTUH-K2044::pKPC-DD02357, NTUH-K2044::pKPC-DD01665, NTUH-K2044::pKPC-DD02201, and NTUH-K2044::pKPC-HS11286), the sodium azide-resistant *E. coli* J53 was used as the recipient. Transconjugants were selected on LB agar plates supplemented with sodium azide (100 μg/mL) and dipotassium tellurite (3 μg/mL). The success of plasmid transfer was confirmed through PCR detection and S1-nuclease pulsed-field gel electrophoresis (S1-PFGE). A CRKp clinical isolate HS11286, which belongs to ST11 and harbours an IncFII$_{K2}$ KPC-2 plasmid, was used for comparison. Conjugation frequency was calculated as the ratio of transconjugants to recipients. The minimum inhibitory concentrations (MICs) of antimicrobial agents were determined using the broth microdilution method following the guidelines provided by the Clinical and Laboratory Standards Institute (CLSI).[20]

Bacterial growth curves and in vitro competition experiment

Bacterial growth was measured in LB broth. Briefly, isolates were cultured overnight in LB broth, diluted to an OD$_{600}$ of 0.01 and grown at 37 °C with shaking (200 rpm). Each isolate was tested in triplicate. The culture cell density was determined every 2 h over a 24-h period by measuring the OD at 600 nm (Thermo Fisher Scientific, Shanghai, China).

In the in vitro competition assays, NTUH-K2044 transconjugants carrying either pKPC-H39 (IncFII$_{K34}$) or pKPC-HS11286 (IncFII$_{K2}$) were cultured overnight in LB broth at 37 °C. The bacteria were diluted to 0.5×10^6 colony-forming units (CFU)/mL, and equal volumes of NTUH-K2044::pKPC-H39 and NTUH-K2044::pKPC-HS11286 were combined and cultured at 37 °C with shaking (200 rpm) in LB containing 1 μg/mL meropenem and LB broth without meropenem,

respectively. At 0, 4, 8, 12, and 24 h, aliquots of the mixed culture were diluted with 0.9% saline solution and plated on LB agar plates with meropenem (0.5 μg/mL). At each time point, 100 colonies were randomly selected from the plate and qPCR targeting the plasmid specific fragments was used to determine the presence of each strain.

Murine intraperitoneal infection model

The mouse intraperitoneal infection assay was conducted as previously described.[21] Briefly, *K. pneumoniae* were grown overnight, and subcultured to logarithmic phase. In the mouse intraperitoneal infection assay, male ICR mice (6–8 weeks old, weighing 20–25 g) were infected intraperitoneally with 10^4 CFUs of *K. pneumoniae* (10 mice/group). The survival of mice was monitored for 7 days. To quantify tissue bacterial burdens, a separate group of mice was intraperitoneally infected with 10^4 CFUs of *K. pneumoniae* (6 mice/group). After 24 h of infection, tissues were collected within 5 min of euthanasia. The lungs, livers, kidneys and spleens were segregated and homogenized with PBS (100 μL PBS/100 mg tissue) by a tissue homogenizer. Bacterial loads were counted by plating serial dilutions on LB agar plates. The hvKp ST23-K1 reference strain *K. pneumoniae* NTUH-K2044 and the non-virulent strain *K. pneumoniae* ATCC 13883 were used as controls. Each experiment was conducted in duplicate.

Proinflammatory cytokine induction assay

For cytokine enzyme-linked immunosorbent assay (ELISA) assay,[21] male ICR mice (6–8 weeks old, weighing 20–25 g) were infected intraperitoneally with 10^5 CFUs of *K. pneumoniae* (12 mice/group) or 100 μl of PBS (3 mice/group as controls). Blood samples were collected at five timepoints post infection (2, 6, 9, 12 h and 24 h), and coagulated at room temperature for 20 min. Supernatants were collected by centrifugation, and the concentrations of TNF-α and IL-6 were determined using the ELISA kits (NeoBioscience, Shenzhen, China) according to the manufacturer's instructions. The hvKp ST23-K1 reference strain *K. pneumoniae* NTUH-K2044 and the non-virulent strain *K. pneumoniae* ATCC 13883 were used as controls. Each experiment was repeated twice with at least three biological replicates. All animal experiments were carried out in accordance with the protocols approved by the Animal Ethics Committee of Huashan Hospital (reference number: 2022-03-HSYY-XXG-34).

Mucoviscosity and biofilm production assays

The mucoviscosity was evaluated through low-speed centrifugation of liquid cultures.[22] Briefly, overnight cultures were centrifuged at 9400 g and resuspended in PBS to an OD_{600} of 1. The suspensions were then centrifuged for 5 min at 1000 g, and the OD_{600} values of the supernatant were measured. These experiments were conducted twice with at least three biological replicates. For biofilm production, 1 μl of an overnight culture was transferred to 100 μl of fresh LB broth in each well of untreated 96-well polystyrene plates and cultured at 37 °C for 5 h. Bacteria were stained with 25 μl of 0.5% crystal violet for 20 min. Then, unbound dye was removed, and the wells were washed three times with water. The biofilm-bound dye was then eluted with 200 μl of 95% ethanol. Absorbance at OD_{595} was measured using a microplate reader to quantify biofilm production.

Anti-neutrophil killing assay

For neutrophil killing assays,[21] neutrophils were isolated from blood of healthy volunteers by density gradient centrifugation with Polymorphprep™, and adjusted to 1×10^7 cell/mL in PBS. Neutrophils (1×10^6) were precultured in flat-bottom plates for 30 min, and incubated with 4×10^7 CFU of opsonized *K. pneumoniae*. Neutrophils were subsequently lysed with 0.1% Triton X-100 on ice for 15 min. Viable bacteria were counted by plating serial dilutions on LB agar. A control experiment without neutrophils was conducted for each *K. pneumoniae* isolate. The bacterial survival rate was calculated as the CFU ratio of experimental group to control group. The hvKp ST23-K1 reference strain *K. pneumoniae* NTUH-K2044 and the non-virulent strain *K. pneumoniae* ATCC 13883 were used as controls. The study was approved by the institutional review board of Huashan Hospital in China (approval no. 2018-461-1) with informed consent obtained from all participants.

Whole genome sequencing and bioinformatic analysis

The whole genomes were sequenced using the HiSeq ×10 Sequencer (Illumina, San Diego, CA, USA) and MinION (Nanopore, Oxford, United Kingdom), and assembled to closure by using Unicycler v0.5.0.[23] Sequence types, capsule types, virulence factors, ICEKp types, and antimicrobial resistance genes were identified by using Kleborate v2.2.0.[24] CRISPR-Cas was identified by using cctyper v1.8.0[25] and anti-CRISPR proteins were detected by BLAST against the AcrDB[26] database. Plasmid replicons were analysed by using PlasmidFinder and plasmid MLST.[27] The phylogenetic tree of plasmid replicon alleles was constructed by using the Neighbour-Joining method in MEGA v11.[28] Circular and linear sequence alignments were plotted by using BRIG v0.95[29] and Easyfig v2.1,[30] respectively. Copy numbers of bla_{KPC-2} and plasmids were analysed by using CCNE v1.1.0.[31]

A total of 342 ST23-K1 genomes were randomly selected for phylogenetic analysis (see Table S1). Recombination events were detected and removed by using Gubbins v3.3.5.[32] A recombination-free phylogenetic tree from Gubbins was visualized with iTOL v5.[33] Date phylogenies were constructed by using BactDating v1.1.[34]

RNA sequencing and differential expression analysis

Overnight cultures of the NTUH-K2044 transconjugants harbouring pKPC-H39 ($IncFII_{K34}$), pKPC-DD02357 ($IncFII_{K34}$) and pKPC-HS11286 ($IncFII_{K2}$) were diluted 1:100 in LB and cultured at 37 °C with shaking until they reach the mid-log-phase. Total RNA was extracted from bacterial cultures using the RNeasy Minikit (Qiagen). Three biological replicates were used for each transconjugant. RNA sequencing was performed on the Illumina Novaseq platform. The sequencing reads were mapped to the NTUH-K2044 chromosome as well as pK2044 and pKPC-H39 sequences by Bowtie2 v2.4.2. Differentially expressed genes were identified by using DESeq v1.18.0 with adjusted P value < 0.05 (Wald test) and fold change >2. The transconjugant NTUH-K2044::pKPC-HS11286 was served as control. Heatmaps were generated by pheatmap v1.0.12 and volcano plots were generated by EnhancedVolcano v1.22.0 in R.

Statistical analysis

Statistical analysis was conducted using R v4.2.3. The Mantel–Cox log-rank test was employed to compare the Kaplan–Meier survival curves and to calculate the associated P values for in vivo studies. For the analysis of proportions, Fisher's exact test was employed. For other comparisons and P value calculations, the t-test was used.

Role of the funding source

The funder of the study had no role in study design, data collection, data analysis, data interpretation, or writing of the report.

Results

Identification of an $IncFII_{K34}$ KPC-2 plasmid in CR-hvKp in China and the global epidemiology of the plasmid in CR-hvKp

A total of 485 CRKp isolates from a recent multi-centre cohort study (CRACKLE-2 China cohort[14]) between July 2017 and July 2018, and 259 CRKp isolates from 11 hospitals in China between July 2018 and January 2019[15] were screened for CR-hvKp. Among the 485 CRKp isolates, three CR-hvKp isolates, belonging to ST23-K1 (DD01665 [ARLG-6634], DD02357 [ARLG-7144], and DD02201 [ARLG-6922]), were identified, which were collected from three different tertiary-care hospitals located in Beijing, Shanghai, and Hangzhou. Among the 259 CRKp isolates, one ST23-K1 CR-hvKp isolate (H39) collected from a hospital in Shanghai was identified. Among the four CR-hvKp isolates, one isolate carried an IncN KPC-2 plasmid, while the other three isolates harboured a nontypeable $IncFII_K$ KPC-2 plasmid (Table 1).

The pMLST analysis classified the nontypeable KPC-2 plasmid as an $IncFII_K$ plasmid, with an $IncFII_K$ allele distinct from the 33 known $IncFII_K$ alleles (ranging from $IncFII_{K1}$ to $IncFII_{K33}$) in the plasmid MLST database (Fig. 1a). This new allele, designated $IncFII_{K34}$, showed 84% sequence coverage and 95% BLASTn identity compared with the most common $IncFII_{K2}$ allele (Fig. 1b). Interestingly, based on the data from the PLSDB, the $IncFII_{K34}$ plasmid exhibited the highest carriage rate of carbapenemase genes (64.9%, 24/37), significantly higher than that observed in other $IncFII_K$ plasmids, including $IncFII_{K2}$ (45.5%, 91/200, $P = 0.033$, Fisher's exact test) and $IncFII_{K1}$ (11.2%, 15/134, $P < 0.001$, Fisher's exact test) plasmids (Fig. 1c). These findings were noteworthy since $IncFII_{K2}$ and $IncFII_{K1}$ are the two most common carbapenemase-encoding plasmids among CRKp.[35]

To explore the epidemiology of carbapenemase-encoding plasmids in CR-hvKp, 67,631 *K. pneumoniae* genomes were downloaded from GenBank, of which 2,343 (3.5%) were ST23, ST86 or ST65 hvKp (Fig. S1). These hvKp genomes were reported from 60 countries, including China (n = 1,003), Singapore (n = 175), Vietnam (n = 123), USA (n = 96) and Ireland (n = 94) (Fig. 1d). ST23 was the most dominant clone accounting for 67% (1,566/2,343) of all the hvKp genomes, followed by ST86 (18%, 417/2,343) and ST65 (15%, 360/2,343) (Fig. 1e).

Among the 2,343 genomes, 414 were identified as CR-hvKp, reported from 24 countries. Of these, 174 genomes (42%) carried a KPC gene (166 were KPC-2), followed by an OXA-48-like gene (30%, 124/414, 109 were OXA-48) and an NDM gene (17%, 72/414, 41 were NDM-1 and 31 were NDM-5). The remainder included IMP (5%, 19/414), VIM (1%, 5/414) and genomes encoding two carbapenemases (5%, 20/414) (Fig. 1f). Geographically, KPC-2 was common in China (n = 72), Singapore (n = 65), and Vietnam (n = 12); OXA-48 was common in Russia (n = 16) and Ireland (n = 72); NDM-5 was common in Bangladesh (n = 23), and OXA-232 was common in Thailand (n = 8). Interestingly, nine genomes reported from Germany encoded both NDM-1 and OXA-48 (Fig. 1d). Among the 414 CR-hvKp genomes, ST23 was the most common, accounting for 73% (303/414), followed by ST65 (16%, 65/414) and ST86 (11%, 46/414).

Among the 174 KPC-encoding genomes out of the 414 global CR-hvKp genomes, $IncFII_{K34}$ KPC plasmid (24%, 42/174) was the most prevalent IncF KPC plasmid, followed by F33 (9%, 16/174) and F35 (8%, 14/174) plasmids (Fig. 1g). The F33 KPC-2 plasmid, a prevalent non-conjugative plasmid, is associated with the ST11 CRKp endemic in China.[36] The non-IncF KPC plasmids primarily include the IncP KPC-2 plasmid (n = 65), which has been reported as a dominant carbapenemase-encoding plasmid in CR-hvKp strains from Singapore.[37] Among the 124 OXA-48-encoding genomes out of the 414 CR-hvKp genomes, the IncL/M OXA-48 plasmid was dominant, detected in 72

Klebsiella pneumoniae	DD01665	DD02201	DD02357	H39
Genome size (bp)	5,460,441	5,533,569	5,464,265	5,451,033
K locus-sequence type	KL1-ST23	KL1-ST23	KL1-ST23	KL1-ST23
Number of plasmids	3	3	3	3
Replicon of bla_{KPC-2} harbouring plasmid [size (bp)]	$IncFII_{K34}$ [94,000]	IncN [62,344]	$IncFII_{K34}$ [103,167]	$IncFII_{K34}$ [114,748]
Replicon of large virulence plasmid [size (bp)]	IncHI1B/IncFIB [228,900]	IncHI1B/IncFIB [234,915]	IncHI1B/IncFIB [229,626]	IncFIB [229,037]
Replicon of other plasmid [size (bp)]	ColRNAI [10,060]	IncFII [97,079]	ColRNAI [9,996]	ColRNAI [10,058]
Antimicrobial resistance associated genes[a]	bla_{KPC-2}	bla_{KPC-2}, bla_{TEM-1B}, $bla_{CTX-M-3}$, *dfrA14*, *qnrS1*, *arr-3*, *aac* (6′)-*Ib-cr*, *qnrB52*, *mph*(A), *sul1*	bla_{KPC-2}, *qnrS1*	bla_{KPC-2}, bla_{TEM-1B}, bla_{SHV-12}, *aac*(3)-*IId*
ompK35/36[b]	WT/WT	WT/WT	WT/WT	WT/WT
Virulence associated genes				
rmpADC[c]	Δ*rmpA*, *rmpD-3*, *rmpC-2*	Δ*rmpA*, *rmpD-3*, *rmpC-2*	*rmpA-2*, *rmpD-3*, *rmpC-2*	*rmpA-2*, *rmpD-28*, *rmpC-2*
rmpA2[c]	Δ*rmpA2*	Δ*rmpA2*	Δ*rmpA2*	Δ*rmpA2*
Aerobactin-ST[c]	AbST1: *iucA1B1C1D1iutA1*	AbST1: *iucA1B1C1D1iutA1*	AbST1: *iucA1B1C1D1iutA1*	AbST1: *iucA1B1C1D1iutA1*
Salmochelin-ST[c]	SmST2: *iroB1C4D1N1*	SmST2-1LV: *iroB1C4D1N1*	SmST2-1LV: *iroB1C4D1N1*	SmST2: *iroB1C4D1N1*
Yersiniabactin-ST[d]	YbST46: *ybt* 1; ICE*Kp10*	YbST46: *ybt* 1; ICE*Kp10*	YbST46-2LV: *ybt* 1; ICE*Kp10* (truncated)	YbST47-1LV: *ybt* 1; ICE*Kp10*
Colibactin-ST[d]	CbST29: *clb* 2	CbST29-1LV: *clb* 2	CbST29: *clb* 2	CbST29-1LV: *clb* 2
CPS mutations	WcaG:Tyr36His; WcaJ:Gly32Leu	CpsAB:Ser91Arg; Wzi:Ser221Ala; Wzc:Val586Asp; Wzy:Leu393Phe; WcaG:Tyr36His	CspAB:Leu173*; WcaG:Tyr36His	WcaG:Tyr36His; WcaJ:Gly32Leu
CRISPR-Cas system	Type I-E	Type I-E	Type I-E	Type I-E
Anti-CRISPR	Δ*acrIE9.2*	*acrIE9.2*	*acrIE9.2*	*acrIE9.2*

WT, wild type. [a]The chromosome borne antimicrobial resistance genes including bla_{SHV-11} and *fosA* were excluded. [b]Reference to *K. pneumoniae* ATCC 13883. [c]Plasmid borne virulence genes. [d]Chromosomal virulence genes.

Table 1: **Genomic features of four KL1-ST23 carbapenem-resistant hypervirulent *Klebsiella pneumoniae*.**

genomes from Ireland and 14 from Russia. Similarly, among the 72 NDM-encoding genomes within the 414 CR-hvKp genomes, the IncX3 NDM plasmid was predominantly found in CR-hvKp genomes from Bangladesh (n = 23) and China (n = 26).

To explore the epidemiology of *K. pneumoniae* genomes harbouring $IncFII_{K34}$ plasmids, we examined data from GenBank and identified 834 genomes harbouring this plasmid, reported from 33 countries (Fig. S2a). Of them, 82% (685/834) were classified as CRKp, 64% (530/834) carried the KPC gene (506 were KPC-2) (Fig. S2b), and 49% (405/834) were classified as ST15 (Fig. S2c). ST23, ST86 and ST65 together accounted for 5% (43/834) of all these genomes. Additionally, the reports of $IncFII_{K34}$ plasmids in *K. pneumoniae* have shown a steady increase from 2003 to 2024 (Fig. S2d).

Genomic features of the CR-hvKp isolates harbouring $IncFII_{K34}$ KPC-2 plasmids and the phylogenetic analysis of hvKp and CR-hvKp strains

Complete genomic analysis revealed that the four CR-hvKp isolates harboured two copies of chromosomal type I-E CRISPR-Cas systems, which commonly target IncF plasmids, and a ~220-Kb, pK2044-like hypervirulence plasmid (Fig. S3). Additionally, isolates DD01665, DD02357, and H39 contained an extra ~100-Kb $IncFII_{K34}$ KPC-2 plasmid that encoded the anti-CRISPR AcrIE9.2 (Fig. 2a), and a ~100-Kb ColRNA plasmid (Fig. S3a–c). The bla_{KPC-2} was located on the NTE_{KPC}-Ib element (Fig. 2b). In contrast, DD02201 harboured a 62-Kb IncN KPC-2 plasmid (Fig. 2c) with the bla_{KPC-2} on the NTE_{KPC}-Id element (Fig. 2d), and a ~97-Kb $IncFII_{K2}$ multidrug-resistance plasmid that encoded AcrIE9.2 (Fig. S3d). AcrIE9.2 has been reported to protect the IncF KPC-2 plasmid from elimination by type I-E CRISPR-Cas system.[38]

Virulence genes, including regulator genes of mucoid phenotype (*rmpADC* and *rmpA2*), aerobactin (*iucABCD*, and *iutA*), and salmochelin (*iroBCDN*), were identified on all the four hypervirulence plasmids. Other virulence genes, including yersiniabactin (*ybt1*; ICE*Kp10*) and colibactin (*clb*), were identified on the chromosomes. Of note, both *rmpA* and *rmpA2* were truncated in DD01665, while *rmpA* was intact and *rmpA2* was truncated in DD02201, DD02357 and H39.

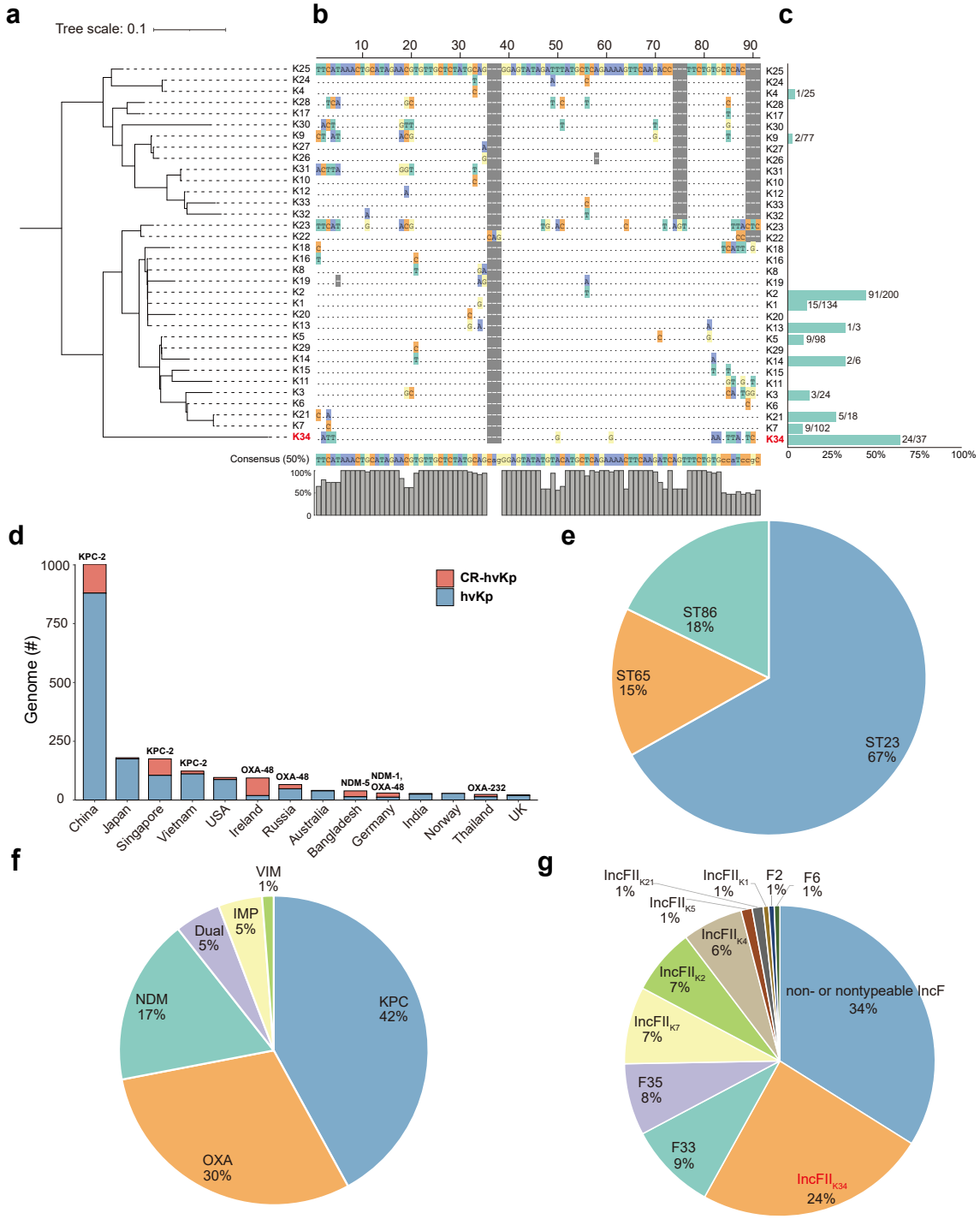

Fig. 1: **Analysis of IncFII$_{K1-34}$ alleles and global epidemiology of CR-hvKp**. **a**. The classification tree for different IncFII$_{K1-34}$ alleles was constructed using the Neighbour-Joining method in MEGA and was rooted at the midpoint. Sequences from the *copA* region of the IncFII$_K$ replicon were used in the tree construction. **b**. The alignment of the IncFII$_{K34}$ allele with 33 known IncFII$_K$ alleles is shown. Dots indicate nucleotides identical to the consensus sequence, and dashes in grey represent gaps. **c**. The proportion of plasmids harbouring carbapenemase-encoding genes in each IncFII$_K$ plasmid type was calculated using data from PLSDB v. 2021_06_23_v2. **d**. The global distribution of 2,168 hvKp and CR-hvKp genomes with country information available from the NCBI GenBank is illustrated. Countries with more than 20 reported hvKp and CR-hvKp genomes were presented, and the predominant carbapenemase type within the country is highlighted on the top of the bar. **e**. The percentages of ST23, ST86, and ST65 among 2,343 hvKp and CR-hvKp strains are presented. **f.** The percentages of carbapenemases found among 414 CR-hvKp strains are detailed. **g.** The distribution of different IncF plasmid replicons among 174 KPC-encoding CR-hvKp strains is depicted.

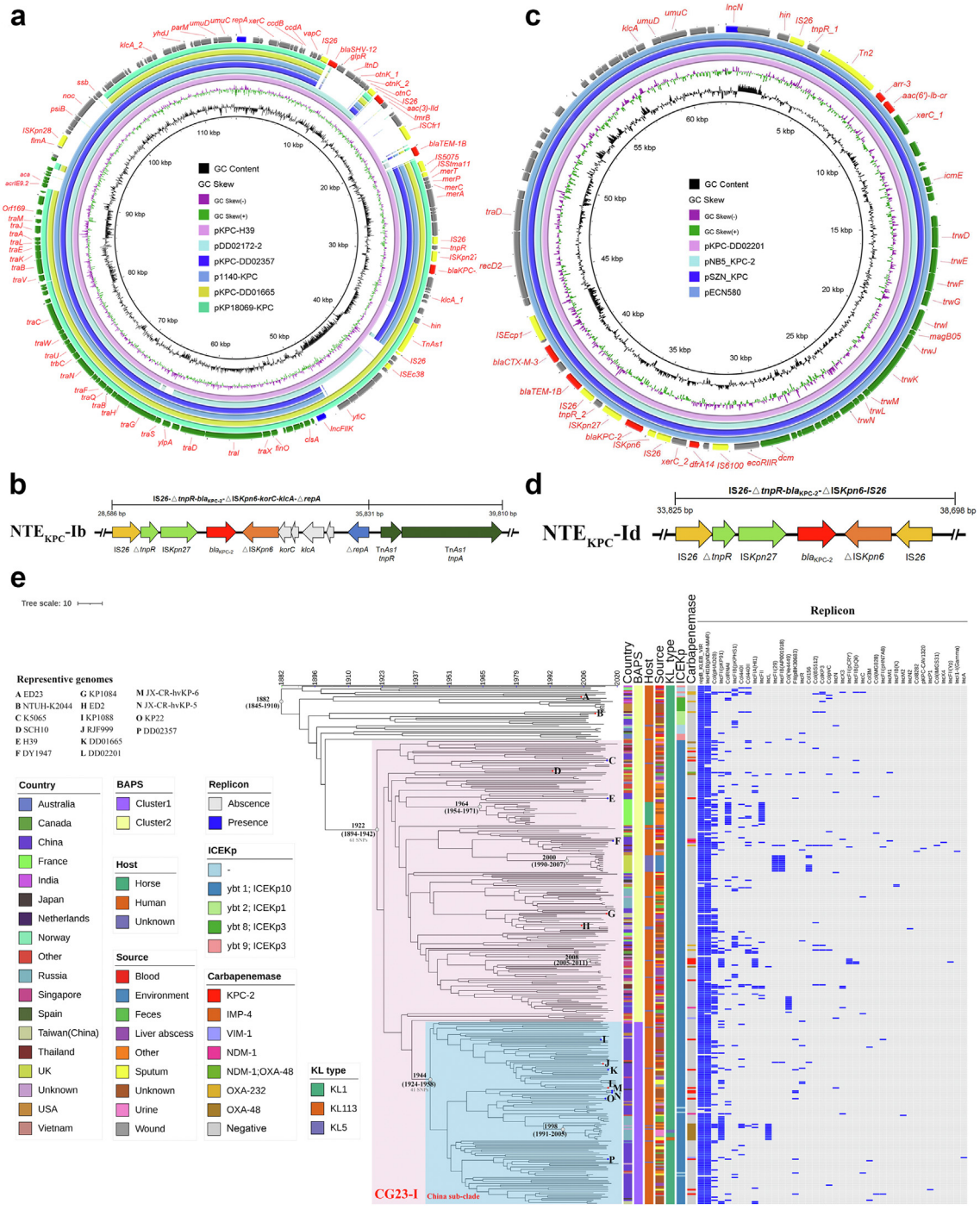

Fig. 2: **Comparative analysis of KPC plasmids in CR-hvKp clinical isolates and phylogenetic analysis of ST23 hvKp and CR-hvKp strains**. **a**. Circular comparison of the three IncFII$_{K34}$ plasmids (pKPC-H39, pKPC-DD02357 and pKPC-DD01665) in CR-hvKp with pDD02172-2 (CP087613), p1140-KPC (CP047689) and pKP18069-KPC (CP059890). **b**. Genetic elements of *bla*$_{KPC-2}$ on IncFII$_{K34}$ plasmid. **c**. Circular comparison of the IncN plasmid (pKPC-DD02201) in CR-hvKp with pNB5_KPC-2 (CP092655), pSZN_KPC (MH917123) and pECN580 (KF914891). **d**. Genetic elements of *bla*$_{KPC-2}$ on IncN plasmid. Open reading frames (ORFs) are indicated by arrows and coloured based on predicted gene function. The replication-associated genes are denoted as blue arrows. Resistance genes are indicated by red arrows, while insertion sequences are shown by yellow arrows. Genes in the conjugation module are shown by green arrows. Other genes are indicated by grey arrows. **e**. Time-based phylogenetic analysis of 342 ST23 hvKp and CR-hvKp strains. Colours in columns illustrate region of origin, BAPS cluster, host, source of isolation, K locus type, ICE type, carbapenemase type and presence of replicons. Selected divergence time and 95% CIs are shown at the nodes. All the representative genomes are complete, and strains with red dots on the graph are hvKp and with blue dots are CR-hvKp. The nine CR-hvKp strains harbouring the IncFII$_{K34}$ *bla*$_{KPC-2}$ plasmids are indicated by black arrows.

Sequence analyses showed that these hypervirulence plasmids exhibited high sequence identity with the prototype virulence plasmid pK2044 (>99.97% BLASTn identity and >98% coverage, accession number: AP006726) (Fig. S4).

To investigate the genomic difference between the $IncFII_{K34}$ bla_{KPC-2} plasmids and published plasmids, we compared these $IncFII_{K34}$ bla_{KPC-2} plasmid sequences to all the complete plasmid sequences from the NCBI. Sequence analyses indicated that pKPC-H39 displayed high sequence identity with the $IncFII_{K34}$ pDD02172-2 (99.97% BLASTn identity and 87% coverage, accession number: CP087613), a bla_{KPC-2} plasmid from ST15 *K. pneumoniae* collected in China in 2017; pKPC-DD02357 was identical to the $IncFII_{K34}$ p1140-KPC plasmid from *Serratia marcescens* collected in China in 2018 (100% identity and 100% coverage, accession number: CP047689); and pKPC-DD01665 showed high sequence similarity with the $IncFII_{K34}$ pKP18069-KPC plasmid from ST15 *K. pneumoniae* collected in China (99.59% identity and 99% coverage, accession number: CP059890) (Fig. 2a). Further genomic analysis of these $IncFII_{K34}$ plasmids showed that the bla_{KPC-2} was embedded on NTE_{KPC}-Ib element,[1] and the main differences were the regions containing genes encoding antimicrobial resistance genes (such as bla_{TEM-1B} and bla_{SHV-12}) (Fig. 2b). The sequence of pKPC-DD02201 was identical to the IncN pNB5_KPC-2 plasmid from ST11 *K. pneumoniae* collected in China in 2017 (100% identity and 100% coverage, accession number: CP092655); and showed high similarity with IncN pSZN_KPC plasmid from ST11 *K. pneumoniae* collected in China in 2015 (99.98% identity and 100% coverage, accession number: MH917123); and IncN pECN580 plasmid from ST131 *Escherichia coli* collected in China (99.98% identity and 100% coverage, accession number: KF914891) (Fig. 2c). The bla_{KPC-2} on IncN plasmids was harboured by the NTE_{KPC}-Id element (Fig. 2d).[16] Furthermore, conjugation modules were identified on both the $IncFII_{K34}$ and IncN plasmids.

Comparative analysis of the $IncFII_{K34}$ KPC-2 plasmids (pKPC-H39, pKPC-DD02357, and pKPC-DD01665) and the $IncFII_{K2}$ KPC-2 plasmid pKPHS2 (pKPC-HS11286 in this study) from *K. pneumoniae* HS11286, one of the most prevalent bla_{KPC-2} vectors among the CRKp lineages,[13] revealed a highly similar backbone (Fig. S5). Both plasmids contained the same bla_{KPC-2} containing the NTE_{KPC}-Ib element[16] and similar conjugation-associated *tra* gene clusters. However, the region containing *traJ* (the primary activator of the *tra* operon), *traM* (relaxosome component), and *oriT* (the origin region of transfer) exhibited significant sequence differences (Fig. S4), implying potential difference in conjugation capabilities.

A total of 342 genomes of ST23-K1 genomes were randomly selected for phylogenetic analysis (Table S1). In a previous study, Lam et al. identified the CG23-I sublineage of ST23, which likely emerged around 1928 after acquiring ICE*Kp10* and subsequently spread globally within humans.[39] Here, we demonstrate that the CG23-I sublineage has become the most extensively disseminated group globally. Temporal phylogenetic analysis indicated that the most recent common ancestors (MRCAs) for the entire ST23 population and the CG23-I sublineage likely emerged around 1882 (95% confidence interval [CI]: 1845–1910) and 1922 (95% CI: 1894–1942), respectively, consistent with the estimates reported in the aforementioned study.[39] Additionally, within the CG23-I sublineage, a regionally distributed sub-clade (China sub-clade) emerged around 1944 (95% CI: 1924–1958), which contains most of the $IncFII_{K34}$ plasmid-harbouring CR-hvKp strains (Fig. 2e). Strains in the China subclade were mainly isolated in China and its neighbouring countries. Notably, CR-hvKp strains harbouring the $IncFII_{K34}$ KPC-2 plasmid exhibited significant phylogenetic distances from each other, indicating that the $IncFII_{K34}$ KPC-2 plasmids were horizontally disseminated among hvKp strains.

High conjugation frequency of $IncFII_{K34}$ KPC-2 plasmids via enhanced expression of transfer genes

Given the sequence differences in the *tra* region, we investigated the conjugation capability of $IncFII_{K34}$ KPC-2 plasmids. Compared with the $IncFII_{K2}$ plasmid, the conjugation frequencies of $IncFII_{K34}$ plasmids were 100 times higher when transferred from three clinical CR-hvKp isolates to *E. coli* J53 (Fig. 3a), and were 100 to 1,000 times higher when transferred from their *E. coli* J53 transconjugants to *K. pneumoniae* NTUH-K2044 (Fig. 3b). Interestingly, the IncN KPC-2 plasmid exhibited a high conjugation frequency (10^{-2}) when transferred from *K. pneumoniae* to *E. coli*, but showed a low conjugation frequency (10^{-7}) when transferred from *E. coli* to *K. pneumoniae*.

The pK2044-like virulence plasmid is typically non-conjugative due to the absence of the *tra* transfer operon. However, a previous study demonstrated that this virulence plasmid can be mobilized with the assistance of a suitable helper plasmid, such as the $IncFII_{K2}$ plasmid pKPC-HS11286.[40] Our findings indicate that the three $IncFII_{K34}$ and the IncN plasmids can indeed serve as helper plasmids, facilitating the mobilization of nonconjugative hypervirulence plasmids at higher transfer frequencies (10^{-5}–10^{-6}) than the $IncFII_{K2}$ KPC-2 plasmid pKPC-HS11286 (10^{-8}) (Fig. 3c). The schematic diagram of the conjugation experiments is shown in Fig. 3d. S1-PFGE plasmid profiles of the CR-hvKp isolates and the transconjugants are shown in Fig. S6, and the MIC data of all the strains are presented in Table S2.

To investigate the molecular mechanism underlying the high conjugation frequencies of $IncFII_{K34}$ plasmids, we conducted RNA-seq analysis on NTUH-K2044 conjugated with $IncFII_{K34}$ (NTUH-K2044::pKPC-H39 and

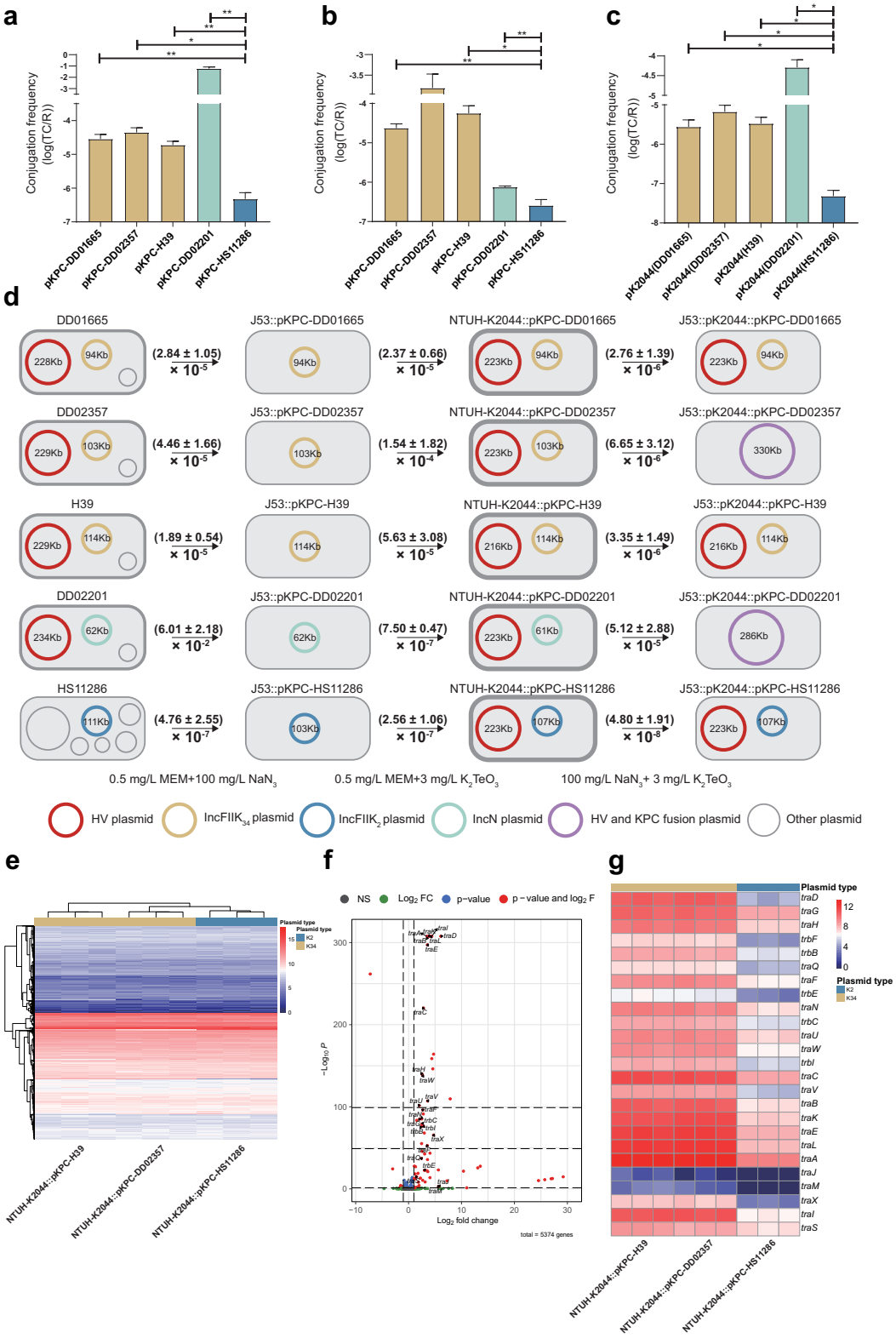

***Fig. 3:* Conjugation assays of bla_{KPC-2} bearing plasmids and RNA-seq analysis of transconjugants**. Conjugation frequencies of KPC-2 plasmids **a** from CR-hvKp or CRKp isolates to *E. coli* J53, and **b** from *E. coli* J53 to *K. pneumoniae* NTUH-K2044. **c**. Conjugation frequencies

NTUH-K2044::pKPC-DD02357) and IncFII$_{K2}$ (NTUH-K2044::pKPC-HS11286) KPC-2 plasmids, respectively (Fig. 3e). The analysis identified 85 (Fig. 3f) differentially expressed genes (DEGs). Among them, 69 DEGs were located on the KPC-2 plasmid, of which 27 conjugation-associated genes were overexpressed in IncFII$_{K34}$ conjugants (Fig. 3g). Besides, 15 DEGs on the chromosome and 1 DEG on the virulence plasmid were identified (Table S3). This expression pattern aligns with the higher conjugation capability observed for the IncFII$_{K34}$ KPC-2 plasmids.

Competitive advantage of IncFII$_{K34}$ KPC-2 plasmid is associated with increased *bla*$_{KPC-2}$ copy numbers and expression in CR-hvKp

To explore factors contributing to the increased prevalence of IncFII$_{K34}$ KPC-2 plasmids in CR-hvKp, we assessed the in vitro fitness of hvKp strains that acquired the KPC-2 plasmids. Specifically, we evaluated the growth of NTUH-K2044 conjugated with either IncFII$_{K34}$ or IncFII$_{K2}$ KPC-2 plasmids at varying meropenem concentrations (0 μg/mL, 0.5 μg/mL, 1 μg/mL, and 2 μg/mL). The MICs of NTUH-K2044 strains conjugated with IncFII$_{K34}$ KPC-2 plasmids to meropenem were 8 μg/mL, while the strain conjugated with the IncFII$_{K2}$ KPC-2 plasmid were 4 μg/mL. Both IncFII$_{K34}$ and IncFII$_{K2}$ KPC-2 plasmids showed minimal impact on NTUH-K2044 growth (Fig. 4a). However, at meropenem concentrations of 0.5 μg/mL (Fig. 4b), 1 μg/mL (Fig. 4c), and 2 μg/mL (Fig. 4d), NTUH-K2044 with IncFII$_{K2}$ exhibited a ~6-h growth lag, whereas those with IncFII$_{K34}$ did not. The competition assays demonstrated that NTUH-K2044 harbouring the IncFII$_{K34}$ KPC-2 plasmid outcompeted those carrying the IncFII$_{K2}$ KPC-2 plasmid in the presence of 1 μg/mL meropenem (Fig. 4e).

Copy number analysis revealed that IncFII$_{K34}$ exhibited elevated *bla*$_{KPC-2}$ (Fig. 4f) and plasmid copy numbers (Fig. 4g) compared with IncFII$_{K2}$ in NTUH-K2044, supporting the competitive advantage of IncFII$_{K34}$ plasmids in CR-hvKp strains. Furthermore, both RNA-seq (Fig. 4h) and qRT-PCR (Fig. 4i) analyses revealed significantly higher expression levels of *bla*$_{KPC-2}$ in NTUH-K2044 harbouring the IncFII$_{K34}$ plasmid compared with those with the IncFII$_{K2}$ plasmid without drug pressure.

Low mucoviscosity observed among CR-hvKp isolates

To determine whether carbapenem resistance affects the pathogenicity of hvKp, we evaluated the in vivo, ex vivo, and in vitro virulence profiles of the four clinical CR-hvKp isolates. The pathogenicity of the ST23-K1 isolates harbouring IncFII$_{K34}$ KPC-2 plasmids, evaluated through assessments of mouse lethality (Fig. 5a), organ invasiveness (Fig. 5b), induction of proinflammatory cytokines (Fig. 5c and d), and resistance to neutrophil-mediated killing (Fig. 5e), was found to be comparable to that of the canonical ST23-K1 hvKp strain, NTUH-K2044. Interestingly, the clinical CR-hvKp isolates, including three harbouring IncFII$_{K34}$ and one with an IncN KPC-2 plasmids, exhibited low mucoviscosity (Fig. 5f) and biofilm formation (Fig. 5g) compared with NTUH-K2044.

To investigate whether carbapenem resistance leads to reduced mucoviscosity in CR-hvKp, we introduced KPC-2 plasmids (IncFII$_{K34,}$ IncN, and IncFII$_{K2}$, as shown in Fig. 3d) into NTUH-K2044. Interestingly, most of the transconjugants showed low mucoviscosity. Overall, the NTUH-K2044 strains conjugated with any KPC plasmid exhibited reduced mucoviscosity, characterized by significantly decreased mean OD$_{600}$ values (Fig. S7). Notably, the mean OD$_{600}$ values of transconjugants carrying IncFII$_{K34}$ plasmids were significantly higher compared with those with IncFII$_{K2}$ plasmids (0.20 vs. 0.12, $P = 0.017$, t-test) or IncN plasmids (0.20 vs. 0.07, $P < 0.001$, t-test). Using an OD$_{600}$ value of less than 0.1 as the cutoff to define low mucoviscosity, the low mucoviscosity rates were 29% (7/24) for NTUH-K2044::pKPC-H39, 46% (11/24) for NTUH-K2044::pKPC-DD02357, 42% (10/24) for NTUH-K2044::pKPC-DD01665, 82% (20/24) for NTUH-K2044::pKPC-DD02201, and 58% (14/24) for NTUH-K2044::pKPC-HS11286. PCR and Sanger sequencing analysis of six colonies with low mucoviscosity from each transconjugant revealed that one NTUH-K2044::pKPC-H39 (IncFII$_{K34}$), one NTUH-K2044::pKPC-DD02357 (IncFII$_{K34}$), and one NTUH-K2044::pKPC-HS11286 (IncFII$_{K2}$) transconjugant had a *rmpA* frameshift or deletion, while no mutations in *wzc* were detected. Whole genome sequencing of the *rmpA* mutated clones observed that the *rmpA* was truncated while *rmpDC* were intact in NTUH-K2044::pKPC-DD02357 and NTUH-K2044::pKPC-HS11286, whereas

of virulence plasmids from *K. pneumoniae* NTUH-K2044 to *E. coli* J53. Three biologic repeats were performed for each strain. Conjugation frequencies are calculated by dividing the number of transconjugants (CFU/mL) by the number of recipients (CFU/mL) and indicated by mean ± SD. *P* values were calculated from student t-tests, $^{*}P < 0.05$, $^{**}P < 0.01$, $^{***}P < 0.001$. **d.** The schematic diagram of the conjugation experiments. The numbers on the arrows are conjugation frequencies. The drugs on the bottom were used for selection in each conjugation experiment. MEM is meropenem, NaN_3 is sodium azide and K_2TeO_3 is potassium tellurite. Only plasmids were shown in the figure. Plasmid profiles were from the results of Nanopore sequencing. The plasmid profile of HS11286 were from the GenBank. **e.** Heatmap of the RNA-seq analysis of NTUH-K2044 conjugated with IncFII$_{K34}$ and IncFII$_{K2}$ KPC-2 plasmids. Three biologic repeats were performed for each strain. **f.** Volcano plot of DEGs between NTUH-K2044 conjugated with IncFII$_{K34}$ and IncFII$_{K2}$ plasmids. **g.** Heatmap of expression of conjugation-associated genes.

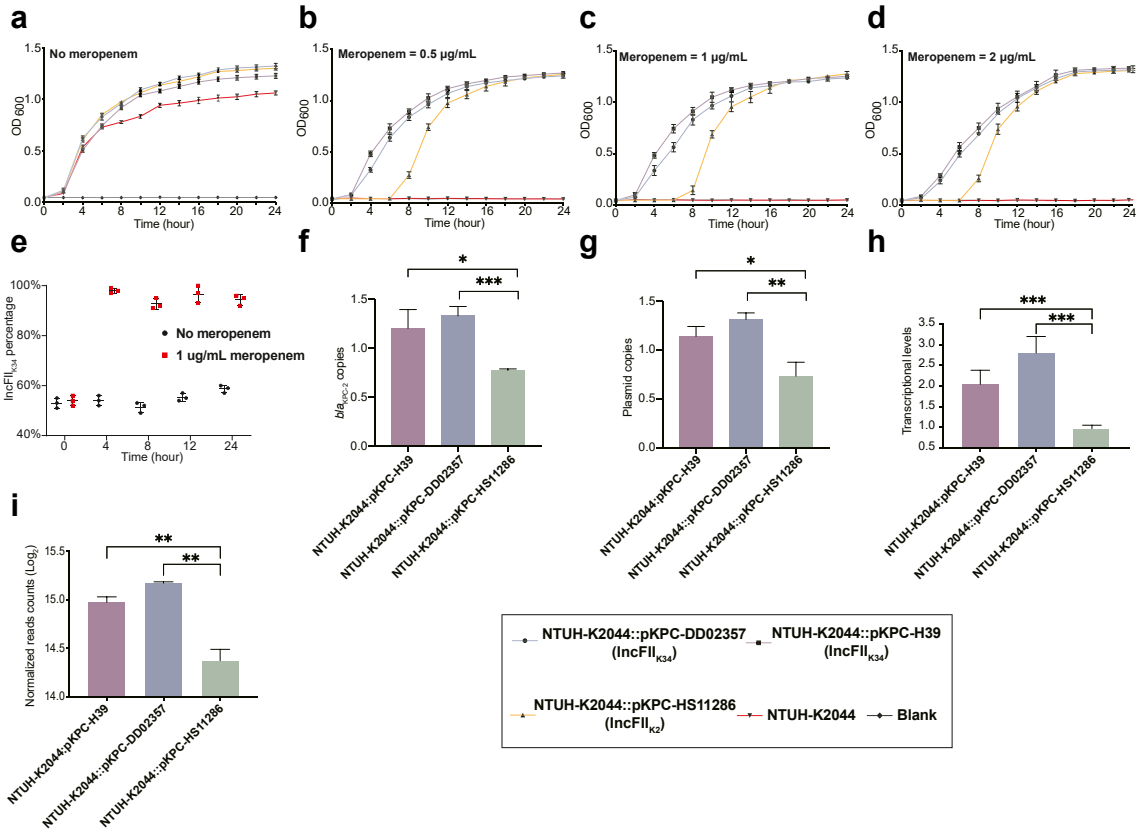

Fig. 4: **The competition experiments of NTUH-K2044 conjugated with IncFII$_{K34}$ and IncFII$_{K2}$ *bla*$_{KPC-2}$ bearing plasmids**. Growth curves of isolates cultured with no meropenem **a**, 0.5 μg/mL meropenem **b**, 1 μg/mL meropenem **c** and 2 μg/mL meropenem **d**. **e**. The competition between isolates under conditions with and without 1 μg/mL meropenem. NTUH-K2044::pKPC-H39 and NTUH-K2044::pKPC-HS11286 were used in the competition assays. The copies of *bla*$_{KPC-2}$ **f** and pKPC-H39, pKPC-DD02357 and pKPC-HS11286 in NTUH-K2044 **g**, respectively. Transcriptional levels of *bla*$_{KPC-2}$ in qRT-PCR **h** and RNA-seq **i**. The transcriptional levels of *bla*$_{KPC-2}$ in qRT-PCR were normalized to the endogenous reference gene *rrsE*. The normalized read counts of *bla*$_{KPC-2}$ in RNA-seq were from the DESeq analysis results. The MICs of NTUH-K2044::pKPC-H39 and NTUH-K2044:: pKPC-DD02357 harbouring IncFII$_{K34}$ KPC-2 plasmids to meropenem were 8 μg/mL, while NTUH-K2044::pKPC-HS11286 with the IncFII$_{K2}$ KPC-2 plasmid were 4 μg/mL. Three biologic repeats were performed for each strain. *P* values were calculated from student t-tests, $^{*}P < 0.05$, $^{**}P < 0.01$, $^{***}P < 0.001$.

the *rmpADC* operon was disrupted by an insertion sequence in NTUH-K2044::pKPC-H39 (Table S4).

The mutation rate of both *rmpADC* and *rmpA2* in CR-hvKp genomes from GenBank was 42% (145/349), significantly higher ($P < 0.001$, Fisher's exact test) than the 18% observed in hvKp genomes without acquired antimicrobial resistance genes (253/1376, odds ratio, 95% CI [3.2, 2.4–4.1]). However, it was significantly lower than the 60% mutation rate observed in ST11 hv-CRKp genomes (2,548/4,240, odds ratio, 95% CI [0.28, 0.22–0.34], $P < 0.001$, Fisher's exact test) that harboured acquired virulence genes *iro* or *iuc*. The most common mutation in *rmpADC* in CR-hvKp was the deletion of the entire operon (48%, 69/145), followed by the deletion or truncation of *rmpA* (41%, 60/145). For *rmpA2* in CR-hvKp, 63% (92/145) were truncated and 37% (53/145) were deleted. ST65 was excluded from the mutation analysis, as nearly all genomes (99.7%, 359/360), including those of CR-hvKp and hvKp, harboured truncated or deleted *rmpADC* and *rmpA2*.

Subsequently, we subjected hypermucoviscous NTUH-K2044 transconjugants (with pKPC-DD01665 or pKPC-DD02201) to 1 μg/mL meropenem treatment for 24 h and found these NTUH-K2044 transconjugants lost their hypermucoviscosity (Fig. S8A and b). Additional incubation of the meropenem treated transconjugants on agar plates identified a mixture of small low mucoviscosity colonies and large hypermucoviscous colonies (Fig. S8c–f). Meropenem time-kill assays found no difference between CR-hvKp with hypermucoviscous and low mucoviscosity phenotypes (Fig. S9). Interestingly, despite the reduction in mucoviscosity, the in vivo virulence of the low mucoviscous transconjugants did not significantly decrease (Fig. S10).

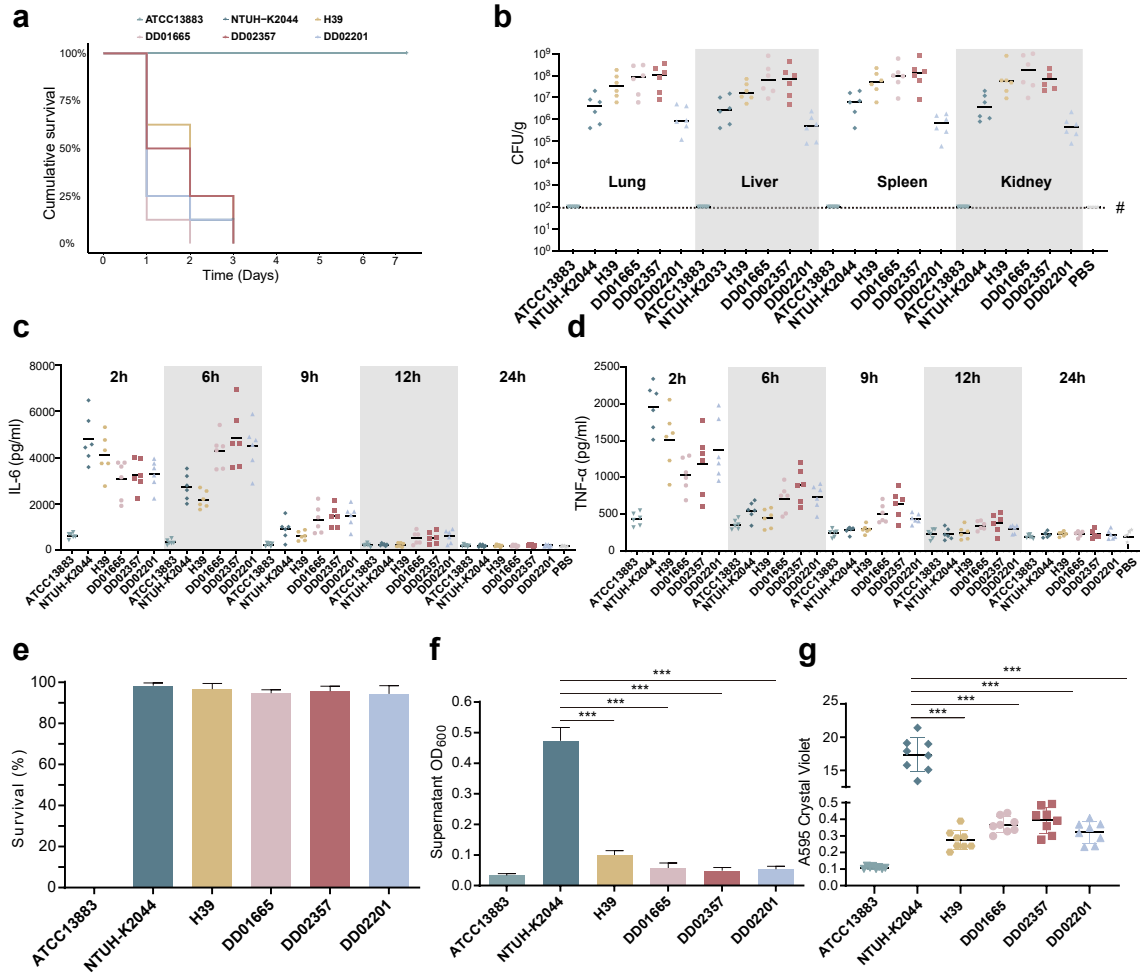

Fig. 5: **The pathogenesis analysis of 4 CR-hvKp isolates**. **a**. Kaplan–Meier survival curves of mice intraperitoneally challenged with *K. pneumoniae* ATCC 13883, NTUH-K2044, H39, DD01665, DD02201 and DD02357. Ten mice for each group were injected with 10^4 CFUs and monitored for 7 days. **b**. Bacterial burdens in the lung, liver, spleen and kidney homogenates of mice. #, the lower limit of detection. Horizontal lines represent median values, and each data point represents an individual mouse. n = 6 per strain. IL-6 **c** and TNF-α **d** of mice serum quantified by ELISA assay. n = 6 per time point per strain. Neutrophil-killing resistance **e**, mucoviscosity **f**, biofilm formation **g** of ATCC13883, NTUH-K2044, H39, DD01665, DD02201 and DD02357. Three biologic repeats were performed for each strain. *P* values were calculated from student t-tests, $^*P < 0.05$, $^{**}P < 0.01$, $^{***}P < 0.001$.

Discussion

Our analysis of public genomic data revealed that hvKp genomes have been identified in 60 countries across all continents, with ST23 being the most dominant lineage, representing 67% of the genomes. Of these, 18% of the genomes, reported from 24 countries, were classified as CR-hvKp, indicating that CR-hvKp has already achieved global distribution. The bla_{KPC} gene was a dominate carbapenemase gene among these CR-hvKp strains, with the $IncFII_{K34}$ plasmid being the prevalent vector.

In this study, we identified an $IncFII_{K34}$ KPC-2 plasmid in *K. pneumoniae* isolates reported from 33 countries. This plasmid exhibited higher expressions of transfer-associated genes, leading to a higher conjugation frequency. Additionally, the plasmid displayed higher copy numbers and expression of bla_{KPC-2}, suggesting a competitive advantage under carbapenem exposure, enabling it to outcompete other plasmids. Notably, clinical CR-hvKp isolates exhibited low mucoviscosity while maintaining hypervirulence, underscoring the need for enhanced molecular diagnostics to accurately detect CR-hvKp. Inadequate laboratory capacity for such diagnostics could lead to an underestimation of the global incidence of hvKp and CR-hvKp.

The increased conjugation frequency significantly promotes plasmid dissemination among bacteria, and plasmid-mediated outbreaks are well-documented.[41] A previous study demonstrated that low fitness costs and

high conjugation frequency contribute to the spread of the IncP KPC-2 plasmid in CR-hvKp strains.[37] In this study, the elevated conjugation frequency of the $IncFII_{K34}$ KPC-2 plasmid, driven by the enhanced expression of conjugation associated genes, likely facilitates its transfer into hvKp strains. Plasmid-mediated antimicrobial resistance also plays a crucial role in plasmid distribution.[41] We observed that the expression levels of bla_{KPC-2} were higher in NTUH-K2044 strains conjugated with $IncFII_{K34}$ KPC-2 plasmids compared with those with $IncFII_{K2}$ KPC-2 plasmids. This increased expression may enable CR-hvKp strains with the $IncFII_{K34}$ KPC-2 plasmid to outcompete others in clinical settings. Furthermore, we found that the carbapenemase-encoding plasmids could act as helper plasmids to facilitate the dissemination of hypervirulence plasmid to other bacteria. Given that hvKp could outcompete other bacteria in the gut,[42] the increasing prevalence of $IncFII_{K34}$ plasmid harbouring CR-hvKp could facilitate the dissemination of hypervirulence plasmid, posing a significant threat to public health and complicating clinical treatment.

Typically, acquisition of antimicrobial resistance genes or plasmids imposes fitness costs on the host.[43] We found that the four clinical CR-hvKp isolates exhibited low mucoviscosity, and most NTUH-K2044 strains conjugated with the KPC-2 plasmids experienced a loss of mucoviscosity. Furthermore, we observed that highly mucoviscous transconjugants lost their mucoviscosity under carbapenem exposure. The reduced mucoviscosity in clinical CR-hvKp isolates and NTUH-K2044 transconjugants was associated with mutations in mucoid regulators. We hypothesized that CR-hvKp may reduce mucoviscosity as a compensatory mechanism to offset the fitness costs associated with acquiring or maintaining carbapenemase-encoding plasmids, with the interference of the mucoid regulator gene *rmpA* being a key mechanism. Hypermucoviscosity provides CR-hvKp with a fitness advantage for invasive infections but incurs a metabolic cost due to the overproduction of CPS.[44] Maintaining both hypervirulence and drug resistance likely imposes a significant burden on CR-hvKp, potentially disadvantaging their survival in hospital settings. The trade-off between CPS biosynthesis and the ability to utilize sufficient energy sources required to resist antibiotic stress may explain the loss of hypermucoviscosity in CR-hvKp strains. Under meropenem treatment, carbapenem resistance becomes the primary factor for survival, leading to the loss of the hypermucoviscosity phenotype as more energy is directed toward resistance mechanisms in CR-hvKp. For example, the acquisition of colistin[45] or tigecycline[46] resistance in hvKp strains leads to reduced capsular production. To offset the fitness cost associated with the acquisition of antimicrobial resistance gene–a critical key factor for bacterial survival in hospital environments–the CR-hvKp likely undergoes compensatory adaptations, such as the loss hypermucoviscosity phenotype.

While hypermucoviscosity has long been regarded as a critical virulence determinant in hvKp, our observations suggest that CR-hvKp strains maintain in vivo virulence and carbapenem resistance even with low mucoviscosity. This finding highlights a significant limitation in the clinical detection of such strains, as the commonly used string test frequently fails to effectively identify these hypervirulent variants.[47] It underscores the need for molecular diagnostics to detect CR-hvKp lacking the hypermucoviscous phenotype in clinical settings. We propose a diagnostic approach incorporating the detection of (a) the 5 plasmid-borne virulence factors including *iucA*, *iroB*, *peg-344*, *rmpA*, and *rmpA2*[48]; (b) key capsular types[49] including wild-type K1 and K2, or sequence types[50] including ST23, ST86 and ST65, and (c) carbapenemase-encoding genes[51] such as bla_{KPC}, $bla_{OXA-48-like}$ and bla_{NDM}, to identify canonical hvKp-derived CR-hvKp strains. Additionally, plasmid multilocus sequence typing[52] can further differentiate carbapenemase-encoding plasmid types. Future research should prioritise global and regional molecular surveillance of CR-hvKp and prevalent carbapenemase gene-encoding plasmids to monitor their spread. These efforts will support the development of infection prevention and control strategies, as well as novel therapies to combat highly resistant and virulent infections. Additionally, tracking the dissemination of $IncFII_{K34}$ KPC plasmids and virulence plasmids across various environments—including the gut microbiome and broader ecological niches—will be crucial in identifying the emergence of other carbapenem-resistant and hypervirulent bacteria.

This study has several limitations. Firstly, it includes only three $IncFII_{K34}$ KPC-2 plasmid-harbouring CR-hvKp clinical isolates in the phenotypic characterisation. Nevertheless, a notable strength of our study is the collection of these CR-hvKp isolates from hospitals across different regions of China. The phylogenetic analysis suggests the independent acquisition of $IncFII_{K34}$ KPC-2 plasmids by different ST23 hvKp strains, supporting the generalizability of our findings. Secondly, while our study primarily compares $IncFII_{K34}$ and $IncFII_{K2}$ KPC-2 plasmids, it is important to acknowledge that other KPC-2 plasmids, as well as plasmids encoding other carbapenemases, may also transfer into hvKp and compete with those carrying the $IncFII_{K34}$ plasmid. Thirdly, the prevalence data inferred from GenBank may not fully reflect the true epidemiological distribution, highlighting the need for expanded molecular surveillance is needed in the future studies.

In conclusion, our findings suggest that the global spread of CR-hvKp may be driven by the $IncFII_{K34}$ KPC-2 plasmids, which we identified in CR-hvKp clinical isolates from China. Despite the loss of hypermucoviscosity, these CR-hvKp strains retain

hypervirulence, posing significant challenges for detection. The global spread of the $IncFII_{K34}$ KPC-2 plasmid underscores the urgent need for coordinated, molecular surveillance of CR-hvKp.

Contributors

JJ collected the genomic data and performed bioinformatics analysis. JJ, LW, YH, and YZ performed experiments. XC and PL conducted AST. JJ and LW wrote the initial draft of the manuscript. LC, XX, JZ, JS and MW critically reviewed the manuscript. DvD, VCF, YD, LC and MW reviewed and revised the manuscript. MW, YX, ZL, YY, and HG served as site leads. MW was responsible for overall study design, and the final manuscript review. JJ, LW and LC have verified the underlying data. All authors were involved with the scientific review and editing of the manuscript. All authors had full access to all the data in the study and had final responsibility for the decision to submit for publication. All authors read and approved the final version of the manuscript.

Data sharing statement

Individual deidentified participant data (and supporting documentation, data dictionaries, and protocol) that underlie the results in this Article can be made available to investigators following submission of a plan for data use, approval by the ARLG or designated entity, and execution of required institutional agreements. Provision might be contingent upon the availability of funding for data preparation and deidentification. More information can be found at https://arlg.org/how-to-apply/request-data/. Sequences are publicly available through the National Center for Biotechnology Information (accession number PRJNA658369 and PRJNA831437).

Declaration of interests

JJ, LW, YH, XC, PL, JZ, YZ, JS, XX, YX, ZL, YY, HG, MW and LC have nothing to declare other than ARLG grant paid to their institution. In addition, and outside of the submitted work the following authors declare the following:

YD reports grants paid to his institution from Entasis and Shionogi; consulting fees paid directly to him from GSK, Meiji Seika Pharma, Shionogi, FujiFilm, AbbVie, Pfizer, and Moderna; and speaker payments from MSD, Shionogi, and Gilead.

DvD reports grants and contracts paid to his institution from the NIH and Merck; consulting fees paid directly to him from Abbvie, Merck, Qpex, Roche, Shionogi, Union, Pfizer, and Utility; honoraria from Clinical Care Options, Entasis, and Pfizer; participation on the Universidade Federal do Rio Grande do Sul Advisory Board and Locus; and an editor's stipend from the British Society for Antimicrobial Chemotherapy (BSAC).

VGF reports grants to his institution from the NIH, MedImmune, Allergan, Pfizer, Advanced Liquid Logics, Theravance, Novartis, Merck, Medical Biosurfaces, Locus, Affinergy, ContraFect, Karius, Genentech, Regeneron, Deep Blue, Basilea, and Janssen; royalties from UpToDate; consulting fees from Novartis, Debiopharm, Genentech, Achaogen, Affinium, Medicines Co., MedImmune, Bayer, Basilea, Affinergy, Janssen, ContraFect, Regeneron, Destiny, Amphliphi Biosciences, Integrated Biotherapeutics, C3J, Armata, Valanbio, Akagera, Aridis, and Roche; editorial stipend from the IDSA; a pending patent for a host gene expression signature diagnostic for sepsis; and stock options with Valanbio and ArcBio.

Acknowledgements

Research reported in this publication was supported by National Natural Science Foundation of China under Award Number 81991531 (MW) and 82102440 (JJ). This study was supported in part by the National Institute of Allergy and Infectious Diseases of the National Institutes of Health (NIAID) under Award Number UM1AI104681. NIAID had no role in the design and conduct of the study; collection, management, analysis, and interpretation of the data; preparation, review, or approval of the manuscript nor the decision to submit the manuscript for publication, or to veto publication, or to control which journal the paper was submitted to. The investigators thank all the patients and their families, and also all contributing clinical microbiology laboratory personnel. The computing power in this work was supported by the National Clinical Research Center for Geriatric Diseases (Huashan Hospital).

Appendix A. Supplementary data

Supplementary data related to this article can be found at https://doi.org/10.1016/j.ebiom.2025.105627.

References

1 Siu LK, Yeh KM, Lin JC, Fung CP, Chang FY. *Klebsiella pneumoniae* liver abscess: a new invasive syndrome. *Lancet Infect Dis*. 2012;12(11):881–887.
2 Wyres KL, Nguyen TNT, Lam MMC, et al. Genomic surveillance for hypervirulence and multi-drug resistance in invasive *Klebsiella pneumoniae* from South and Southeast Asia. *Genome Med*. 2020;12(1):11.
3 WHO. Antimicrobial resistance, hypervirulent *Klebsiella pneumoniae* - global situation. https://www.who.int/emergencies/disease-outbreak-news/item/2024-DON527; 2024.
4 DeLeo FR, Porter AR, Kobayashi SD, et al. Interaction of multidrug-resistant hypervirulent *Klebsiella pneumoniae* with components of human innate host defense. *mBio*. 2023;14:e0194923.
5 Yang X, Sun Q, Li J, et al. Molecular epidemiology of carbapenem-resistant hypervirulent *Klebsiella pneumoniae* in China. *Emerg Microbes Infect*. 2022;11(1):841–849.
6 Wyres KL, Wick RR, Judd LM, et al. Distinct evolutionary dynamics of horizontal gene transfer in drug resistant and virulent clones of *Klebsiella pneumoniae*. *PLoS Genet*. 2019;15(4):e1008114.
7 Tian D, Liu X, Chen W, et al. Prevalence of hypervirulent and carbapenem-resistant *Klebsiella pneumoniae* under divergent evolutionary patterns. *Emerg Microbes Infect*. 2022;11(1):1936–1949.
8 Zhou Y, Tang Y, Fu P, et al. The type I-E CRISPR-Cas system influences the acquisition of bla_{KPC}-IncF plasmid in *Klebsiella pneumonia*. *Emerg Microbes Infect*. 2020;9(1):1011–1022.
9 Karlsson M, Stanton RA, Ansari U, et al. Identification of a carbapenemase-producing hypervirulent *Klebsiella pneumoniae* isolate in the United States. *Antimicrob Agents Chemother*. 2019;63(7):e00519.
10 Mataseje LF, Boyd DA, Mulvey MR, Longtin Y. Two hypervirulent *Klebsiella pneumoniae* isolates producing a bla_{KPC-2} carbapenemase from a Canadian patient. *Antimicrob Agents Chemother*. 2019;63(7):e00517.
11 Chen Y, Marimuthu K, Teo J, et al. Acquisition of plasmid with carbapenem-resistance gene bla_{KPC2} in hypervirulent *Klebsiella pneumoniae*, Singapore. *Emerg Infect Dis*. 2020;26(3):549–559.
12 Yan R, Lu Y, Zhu Y, et al. A sequence type 23 Hypervirulent *Klebsiella pneumoniae* strain presenting carbapenem resistance by acquiring an IncP1 bla_{KPC-2} plasmid. *Front Cell Infect Microbiol*. 2021;11:641830.
13 Beyrouthy R, Dalmasso G, Birer A, Robin F, Bonnet R. Carbapenem resistance conferred by OXA-48 in K2-ST86 hypervirulent *Klebsiella pneumoniae*, France. *Emerg Infect Dis*. 2020;26(7):1529–1533.
14 Mukherjee S, Naha S, Bhadury P, et al. Emergence of OXA-232-producing hypervirulent *Klebsiella pneumoniae* ST23 causing neonatal sepsis. *J Antimicrob Chemother*. 2020;75(7):2004–2006.
15 Xie M, Yang X, Xu Q, et al. Clinical evolution of ST11 carbapenem resistant and hypervirulent *Klebsiella pneumoniae*. *Commun Biol*. 2021;4(1):650.
16 Chen L, Mathema B, Chavda KD, DeLeo FR, Bonomo RA, Kreiswirth BN. Carbapenemase-producing *Klebsiella pneumoniae*: molecular and genetic decoding. *Trends Microbiol*. 2014;22(12):686–696.
17 Wang M, Earley M, Chen L, et al. Clinical outcomes and bacterial characteristics of carbapenem-resistant *Klebsiella pneumoniae* complex among patients from different global regions (CRACKLE-2): a prospective, multicentre, cohort study. *Lancet Infect Dis*. 2022;22(3):401–412.
18 Hu Y, Jiang J, Wang D, Guo Q, Wang M. Coexistence of bla_{KPC}-IncFII plasmids and type I-E* CRISPR-Cas systems in ST15 *Klebsiella pneumoniae*. *Front Microbiol*. 2023;14:1125531.
19 Schmartz GP, Hartung A, Hirsch P, et al. PLSDB: advancing a comprehensive database of bacterial plasmids. *Nucleic Acids Res*. 2022;50(D1):D273–D278.

20 Pitt ME, Elliott AG, Cao MD, et al. Multifactorial chromosomal variants regulate polymyxin resistance in extensively drug-resistant *Klebsiella pneumoniae*. *Microb Genom*. 2018;4(3):e000158.
21 Ye M, Liao C, Shang M, et al. Reduced virulence and enhanced host adaption during antibiotics therapy: a story of a within-host carbapenem-resistant *Klebsiella pneumoniae* sequence type 11 evolution in a patient with a serious scrotal abscess. *mSystems*. 2022;7:e0134221.
22 Walker KA, Miner TA, Palacios M, et al. A *Klebsiella pneumoniae* regulatory mutant has reduced capsule expression but retains hypermucoviscosity. *mBio*. 2019;10(2):e00089.
23 Wick RR, Judd LM, Gorrie CL, Holt KE. Unicycler: resolving bacterial genome assemblies from short and long sequencing reads. *PLoS Comput Biol*. 2017;13(6):e1005595.
24 Lam MMC, Wick RR, Watts SC, Cerdeira LT, Wyres KL, Holt KE. A genomic surveillance framework and genotyping tool for *Klebsiella pneumoniae* and its related species complex. *Nat Commun*. 2021;12(1):4188.
25 Russel J, Pinilla-Redondo R, Mayo-Munoz D, Shah SA, Sorensen SJ. CRISPRCasTyper: Automated identification, annotation, and classification of CRISPR-Cas loci. *CRISPR J*. 2020;3(6):462–469.
26 Huang L, Yang B, Yi H, et al. AcrDB: a database of anti-CRISPR operons in prokaryotes and viruses. *Nucleic Acids Res*. 2021;49(D1):D622–D629.
27 Carattoli A, Zankari E, Garcia-Fernandez A, et al. *In silico* detection and typing of plasmids using PlasmidFinder and plasmid multilocus sequence typing. *Antimicrob Agents Chemother*. 2014;58(7):3895–3903.
28 Kumar S, Stecher G, Li M, Knyaz C, Tamura K, Mega X. Molecular evolutionary genetics analysis across computing platforms. *Mol Biol Evol*. 2018;35(6):1547–1549.
29 Alikhan NF, Petty NK, Ben Zakour NL, Beatson SA. BLAST Ring Image Generator (BRIG): simple prokaryote genome comparisons. *BMC Genomics*. 2011;12:402.
30 Sullivan MJ, Petty NK, Beatson SA. Easyfig: a genome comparison visualizer. *Bioinformatics*. 2011;27(7):1009–1010.
31 Jiang J, Chen L, Chen X, et al. Carbapenemase-encoding gene copy number estimator (CCNE): a tool for carbapenemase gene copy number estimation. *Microbiol Spectr*. 2022;10:e0100022.
32 Croucher NJ, Page AJ, Connor TR, et al. Rapid phylogenetic analysis of large samples of recombinant bacterial whole genome sequences using Gubbins. *Nucleic Acids Res*. 2015;43(3):e15.
33 Letunic I, Bork P. Interactive Tree of Life (iTOL) v5: an online tool for phylogenetic tree display and annotation. *Nucleic Acids Res*. 2021;49(W1):W293–W296.
34 Didelot X, Croucher NJ, Bentley SD, Harris SR, Wilson DJ. Bayesian inference of ancestral dates on bacterial phylogenetic trees. *Nucleic Acids Res*. 2018;46(22):e134.
35 Bi D, Zheng J, Li JJ, et al. *In silico* typing and comparative genomic analysis of $IncFII_K$ plasmids and insights into the evolution of replicons, plasmid backbones, and resistance determinant profiles. *Antimicrob Agents Chemother*. 2018;62(10):e00764.
36 Xiang DR, Li JJ, Sheng ZK, et al. Complete sequence of a novel IncR-F33:A-:B- plasmid, pKP1034, harboring *fosA3*, bla_{KPC-2}, $bla_{CTX-M-65}$, bla_{SHV-12}, and *rmtB* from an epidemic *Klebsiella pneumoniae* sequence type 11 strain in China. *Antimicrob Agents Chemother*. 2015;60(3):1343–1348.
37 Yong M, Chen Y, Oo G, et al. Dominant carbapenemase-encoding plasmids in clinical Enterobacterales isolates and hypervirulent *Klebsiella pneumoniae*, Singapore. *Emerg Infect Dis*. 2022;28(8):1578–1588.
38 Wang C, Sun Z, Hu Y, Li D, Guo Q, Wang M. A novel anti-CRISPR AcrIE9.2 is associated with dissemination of bla_{KPC} plasmids in *Klebsiella pneumoniae* sequence type 15. *Antimicrob Agents Chemother*. 2023;67(4):e0154722.
39 Lam MMC, Wyres KL, Duchene S, et al. Population genomics of hypervirulent *Klebsiella pneumoniae* clonal-group 23 reveals early emergence and rapid global dissemination. *Nat Commun*. 2018;9(1):2703.
40 Liu P, Li P, Jiang X, et al. Complete genome sequence of *Klebsiella pneumoniae* subsp. *pneumoniae* HS11286, a multidrug-resistant strain isolated from human sputum. *J Bacteriol*. 2012;194(7):1841–1842.
41 Alonso-Del Valle A, Toribio-Celestino L, Quirant A, et al. Antimicrobial resistance level and conjugation permissiveness shape plasmid distribution in clinical enterobacteria. *Proc Natl Acad Sci U S A*. 2023;120(51):e2314135120.
42 Hsieh PF, Lu YR, Lin TL, Lai LY, Wang JT. *Klebsiella pneumoniae* type VI secretion system contributes to bacterial competition, cell invasion, type-1 fimbriae expression, and in vivo colonization. *J Infect Dis*. 2019;219(4):637–647.
43 Wyres KL, Lam MMC, Holt KE. Population genomics of *Klebsiella pneumoniae*. *Nat Rev Microbiol*. 2020;18(6):344–359.
44 Mike LA, Stark AJ, Forsyth VS, et al. A systematic analysis of hypermucoviscosity and capsule reveals distinct and overlapping genes that impact *Klebsiella pneumoniae* fitness. *PLoS Pathog*. 2021;17(3):e1009376.
45 Choi MJ, Ko KS. Loss of hypermucoviscosity and increased fitness cost in colistin-resistant *Klebsiella pneumoniae* sequence type 23 strains. *Antimicrob Agents Chemother*. 2015;59(11):6763–6773.
46 Park S, Lee H, Shin D, Ko KS. Change of hypermucoviscosity in the development of tigecycline resistance in Hypervirulent *Klebsiella pneumoniae* sequence type 23 strains. *Microorganisms*. 2020;8(10):1562.
47 Russo TA, Olson R, Fang CT, et al. Identification of biomarkers for differentiation of hypervirulent *Klebsiella pneumoniae* from classical *K. pneumoniae*. *J Clin Microbiol*. 2018;56(9):e00776.
48 Russo TA, Alvarado CL, Davies CJ, et al. Differentiation of hypervirulent and classical *Klebsiella pneumoniae* with acquired drug resistance. *mBio*. 2024;15(2):e0286723.
49 Yu F, Lv J, Niu S, et al. Multiplex PCR analysis for rapid detection of *Klebsiella pneumoniae* carbapenem-resistant (Sequence Type 258 [ST258] and ST11) and hypervirulent (ST23, ST65, ST86, and ST375) strains. *J Clin Microbiol*. 2018;56(9):e00731.
50 Diancourt L, Passet V, Verhoef J, Grimont PA, Brisse S. Multilocus sequence typing of *Klebsiella pneumoniae* nosocomial isolates. *J Clin Microbiol*. 2005;43(8):4178–4182.
51 Monteiro J, Widen RH, Pignatari AC, Kubasek C, Silbert S. Rapid detection of carbapenemase genes by multiplex real-time PCR. *J Antimicrob Chemother*. 2012;67(4):906–909.
52 Villa L, Garcia-Fernandez A, Fortini D, Carattoli A. Replicon sequence typing of IncF plasmids carrying virulence and resistance determinants. *J Antimicrob Chemother*. 2010;65(12):2518–2529.